

Making high-quality quantum microwave devices with van der Waals superconductors

Abhinandan Antony,¹ Martin V. Gustafsson,² Anjaly Rajendran,³ Avishai Benyamini,¹ Guilhem Ribeill,² Thomas A. Ohki,² Takashi Taniguchi,⁴ Kenji Watanabe,⁵ James Hone,¹ and Kin Chung Fong^{2, a)}

¹⁾*Department of Mechanical Engineering, Columbia University, New York, NY 10027, USA*

²⁾*Raytheon BBN Technologies, Quantum Engineering and Computing Group, Cambridge, Massachusetts 02138, USA*

³⁾*Department of Electrical Engineering, Columbia University, New York, NY 10027, USA*

⁴⁾*International Center for Materials Nanoarchitectonics, National Institute for Materials Science, Tsukuba, Japan*

⁵⁾*Research Center for Functional Materials, National Institute for Materials Science, Tsukuba, Japan*

(Dated: 1 April 2025)

Ultra low-loss microwave materials are crucial for enhancing quantum coherence and scalability of superconducting qubits. Van der Waals (vdW) heterostructure is an attractive platform for quantum devices due to the single-crystal structure of the constituent two-dimensional (2D) layered materials and the lack of dangling bonds at their atomically sharp interfaces. However, new fabrication and characterization techniques are required to determine whether these structures can achieve low loss in the microwave regime. Here we report the fabrication of superconducting microwave resonators using NbSe₂ that achieve a quality factor $Q > 10^5$. This value sets an upper bound that corresponds to a resistance of $\leq 192\mu\Omega$ when considering the additional loss introduced by integrating NbSe₂ into a standard transmon circuit. This work demonstrates the compatibility of 2D layered materials with high-quality microwave quantum devices.

Fault-tolerant quantum computation requires qubits with long coherence times^{1,2}. Over the past two decades, researchers have increased the lifetimes of superconducting qubits by orders of magnitude, in large part by improving their geometries and constituent materials to reduce microwave losses^{3,4}. In parallel with these advances, stacked van der Waals (vdW) materials have emerged as a platform of wide applicability, enabling new devices such as gate-tunable qubits⁵ and resonators⁶, and single-photon detectors⁷. Because the vdW flakes are fabricated by cleaving pristine crystals, we could reduce the number of defects and contamination both on the surfaces and in the bulk, thus potentially improving the qubit coherence. However, the use of vdW superconductors such as niobium diselenide (NbSe₂), tungsten ditelluride (WTe₂), and tantalum disulphide (TaS₂), in quantum devices has remained largely unexplored. While the existing fabrication techniques have proven to be sufficient to achieve good DC transport measurement characteristics, the same process does not directly apply to quantum devices. For instance, the dielectric loss in microwave frequencies at the single-photon limit, rather than the DC loss measured at high power, determines the performance of superconducting qubits; a finite electrical contact resistance⁸ is acceptable in DC transport, but detrimental to quantum devices. Moreover, superconductors in the 2D limit may have additional loss channels due to reduced superfluid stiffness⁹, unpaired vortices^{10,11}, as well as spin-orbit coupling¹². To use vdW superconductors in low-loss microwave circuits, it is necessary to integrate them with conventionally fabricated

superconductors to produce high-quality factor resonators and long-coherence time qubits.

Here, we present the integration of exfoliated NbSe₂ flakes and deposited Al into a monolithic superconducting microwave platform. We verify a method to fabricate transparent contacts between the two materials and confirm that the incorporation of NbSe₂ in our circuit does not introduce excess microwave dissipation. This development paves the way for more complex quantum microwave circuits that take advantage of the unique features of vdW superconductors, such as compact transmon qubits^{13,14} with stacked parallel-plate capacitors¹⁵.

Our process of combining NbSe₂ with conventional superconductors to make high- Q microwave resonators starts with a high resistivity silicon substrate sputter-coated with 200 nm of niobium. Resonators are made from the Nb film by photolithography and plasma etching. At the end of each resonator, a $400\mu\text{m} \times 400\mu\text{m}$ area of bare Si is left open for the placement of vdW flakes or heterostructures. The use of pre-patterned Nb films reduces the risk of getting polymer residue from the vdW materials deposition trapped between the metal film and the substrate. Inside a glove box filled with nitrogen gas, we exfoliate NbSe₂ flakes onto a silicon wafer with 285 nm of SiO₂ on the top. The thickness of NbSe₂ flakes are on the order of 35 nm, initially selected by their optical contrast and later confirmed with an atomic force microscope. We use a polypropylene carbonate (PPC)/Polydimethylsiloxane (PDMS) based dry-pick-up and transfer process¹⁶ to transfer selected flakes onto the uncovered silicon areas on the patterned resonator substrates. During this process, care is taken to restrict the size of the contact area between the PPC/PDMS stamp and the substrate. Finally, we use e-beam lithography to define an electrode pattern that connects the NbSe₂ to the

^{a)}Electronic mail: kc.fong@raytheon.com

Nb, and also extends the ground plane into the region near the vdW stack (Fig. 1a).

Upon contact with air, a layer of native oxide inevitably forms on the outer surfaces of the NbSe₂¹⁷. To remove this oxide layer and ensure superconducting contact, we use in-situ argon ion milling prior to metal deposition to remove the surface layers of the materials exposed through the resist mask¹⁸. The milling is deep enough such that both a horizontal surface and a vertical edge of the NbSe₂ flake are available for metal contact. Without breaking vacuum, we deposit an adhesion layer of Ti (3 nm) followed by a Al (typically 70 - 120 nm) over the freshly exposed surfaces, followed by lift-off in acetone, thereby completing the contact between Al and NbSe₂ as well as between Al and Nb.

To confirm the effectiveness of this technique, we perform cross-sectional energy-dispersive spectroscopy (EDS) (Fig. 1b-e). We find that the NbSe₂ under the Al contact (Fig. 1b)

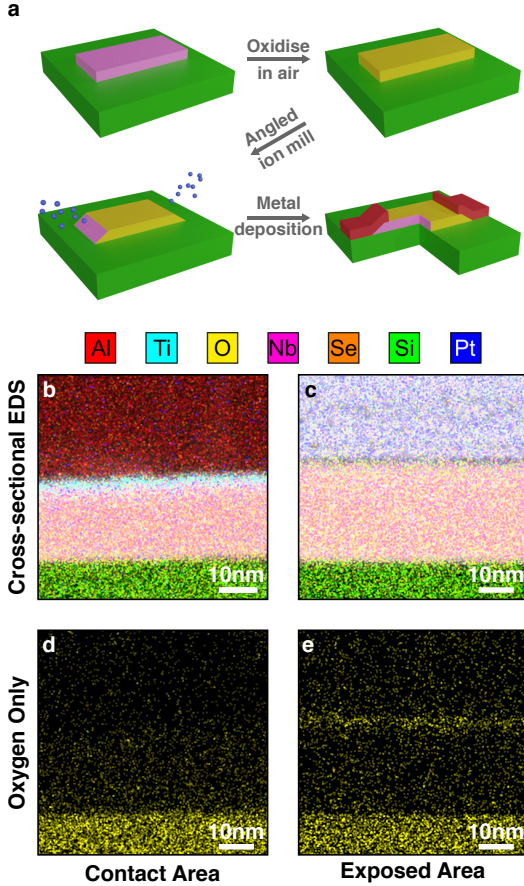


FIG. 1. Fabrication process and cross-sectional energy-dispersive spectroscopy (EDS). (a) NbSe₂ is transferred onto a pre-patterned void in the ground plane made of niobium on a silicon chip (top left). The surface of NbSe₂ is oxidized upon exposure to air (top right). Argon ion milling is performed at an angle (bottom left) exposing pristine NbSe₂ and contacts are then deposited in the same chamber without exposure to air (bottom right). (b) and (c) False color cross sectional EDS maps of the contacts and exposed areas, respectively. (d) and (e) Contribution of oxygen to each of the above maps.

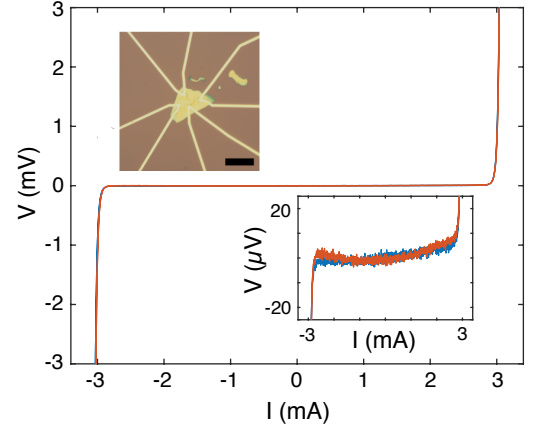


FIG. 2. DC characteristics. Voltage V versus bias current I across two NbSe₂-Al contacts, showing pronounced switching to a resistive state at $I \approx 3$ mA. Data for two pairs of contacts are included in the plot and they fall on top of each other. The lower inset shows a zoom-in (blue and orange), with a constant voltage offset subtracted from each. For currents below the transition threshold, we observe no signs of electrical resistance. The drift near zero voltage can be attributed to limitations in the DC instrumentation. Top-left inset: optical image of the device used in the DC measurement. The black scale bar is 20 μm long.

is thinner by about 5 nm than in other areas (Fig. 1c) due to the ion milling. By highlighting the oxygen content (Fig. 1d and e), we can see a layer with a high concentration of oxygen atoms near the surface of NbSe₂ that has been exposed to the air, which is absent in NbSe₂ that has been covered by Al.

To confirm that there is an electrical contact to NbSe₂, we fabricate test devices for DC measurement using the fabrication procedures described above (Fig. 2 top-left inset). Measuring the resistance through two contacts in series at a temperature of 25 mK, we find no observable resistance in the I-V characteristic for currents lower than ~ 3 mA. Below this threshold, we measure a variation in voltage lower than 10 μV , and attribute the drift to limitations in our instrument (bottom-right inset). The sharp voltage rise at ~ 3 mA can be due to the bias current exceeding the critical current density of Al superconductor electrodes or of the Josephson junction formed between the NbSe₂-Al contact. For a 107 nm thick, 2 μm wide Al electrode, the transition would correspond to a critical current density of 14 GA/m², smaller than but consistent with the value from other reports¹⁹. On the other hand, if this sharp voltage increase is due to the bias current exceeding the critical current I_c of a Josephson junction formed at the contact, we can estimate the normal-state tunneling resistance of the junction, R_N , using Ambegaokar-Baratoff formula²⁰: $R_N = \pi\Delta/2eI_c$, with Δ and e being the superconducting gap energy and electron charge, respectively. Using superconducting gap values for Al and NbSe₂ of 0.23 and 1.1 meV, respectively, and $\Delta = 2\Delta_{\text{Al}}\Delta_{\text{NbSe}_2}/(\Delta_{\text{Al}} + \Delta_{\text{NbSe}_2})$ ²¹, we find $R_N = 0.2\Omega$ if $I_c = 3$ mA. This would imply a voltage drop of 0.6 mV. Since the joule heating is large, on the order of μW , at the transition, we cannot determine the nature of this transition except confirming a dissipationless contact up to a DC

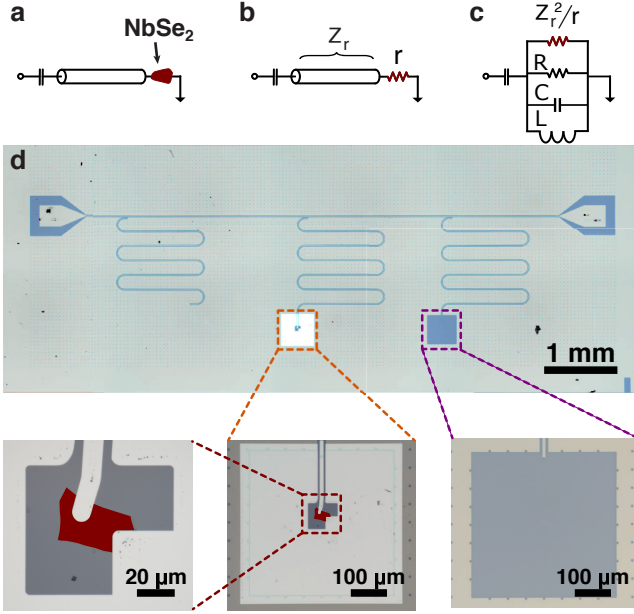


FIG. 3. Circuit diagram and optical micrographs. (a) Schematic of the circuit of the quarter-wave resonator terminated to ground with a NbSe₂ flake. (b) Model representation of the loss caused by the NbSe₂ flake and its contacts. (c) Equivalent circuit for the terminated resonator shown in (b). (d) Optical micrographs of a representative device, showing the reference (left), quarter-wave (middle) and control (right) resonators, and enlarged images of the NbSe₂ termination and the control resonator.

bias current of ~ 3 mA.

By testing superconducting resonators with embedded NbSe₂, we are able to verify that the NbSe₂/Al system is suitable for quantum microwave devices. Since the non-NbSe₂ parts of the resonators are fabricated in a process that is capable of yielding high quality factors, the superconducting resonators can serve as sensitive probes for any microwave losses introduced by the NbSe₂ flake or its contacts^{22,23}, which manifest as a degradation of the resonator's internal quality factor Q_i . Fig. 3a shows a schematic of the resonator, with the NbSe₂ shunting one end of a capacitively coupled coplanar waveguide (CPW) to ground, thus forming a quarter-wave resonator. We can model the loss associated with the NbSe₂ flake as a resistor r (Fig. 3b) and represent the entire quarter-wave resonator as a parallel RLC circuit with R , L , and C representing the resistive loss, inductance, and capacitance of the CPW resonator (Fig. 3c). For a characteristic CPW impedance Z_r and resonance frequency of $\omega_0/2\pi$, Q_i is given by:

$$Q_i = \omega_0 \left(\frac{1}{R} + \frac{r}{Z_r^2} \right)^{-1} C \quad (1)$$

$$\frac{1}{Q_i} = \frac{1}{Q_0} + \frac{r}{\omega_0 C Z_r^2} \quad (2)$$

Here, Q_0 is the internal quality factor of the CPW part of the resonator, modeled by the resistance R . In this circuit model, the loss of the NbSe₂ flake acts as a shunt resistance of value Z_r^2/r .

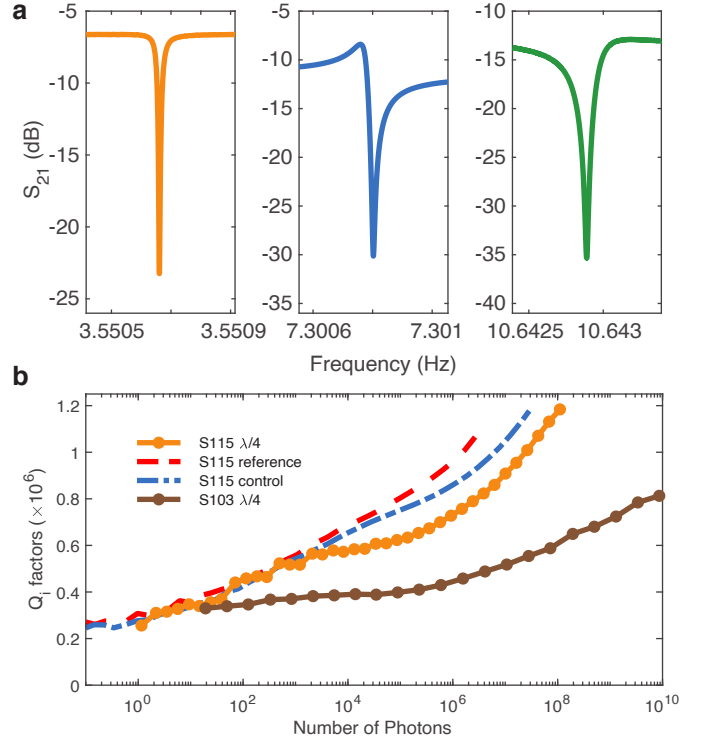


FIG. 4. High frequency loss measurements (a) Transmitted amplitude vs frequency for fundamental (orange) and first harmonic (green) modes of the quarter wave resonator, and control resonator (blue). (b) Internal quality factor vs the number of photons from the applied power for the fundamental mode of quarter wave resonators for two devices, as well as the reference and control of one of them for comparison.

Fig. 3d shows optical images of one of our devices, with three meandered CPW resonators capacitively coupled to a CPW feed line running through the center of the chip. The leftmost resonator is made entirely from Nb and serves as a benchmark for the fabrication process and the experimental setup. For the two resonators to the right, the Nb patterns are geometrically identical and end in open areas of bare Si where a vdW flake can be placed. In one of these two resonators, we short the end of CPW to ground through a flake of NbSe₂ to create a quarter-wave resonator with center frequency $\omega_{\lambda/4}$. The other one (Fig. 3d) is left unmodified and serves as a control resonator with resonance frequency $\omega_{\lambda/2} \approx 2\omega_{\lambda/4}$.

Fig. 4a shows the resonances of the quarter-wave and control resonators as notches in the transmission spectrum through the CPW feedline. The fundamental mode of the quarter-wave and control resonators are at $\omega_{\lambda/4}/2\pi = 3.551$ GHz and $\omega_{\lambda/2}/2\pi = 7.301$ GHz, respectively. The resonance frequency of the control resonator is slightly higher than twice the quarter-wave resonance frequency because of the Al extension that couples the NbSe₂ and the Nb CPW. The resonance near $3\omega_{\lambda/4}/2\pi = 10.643$ GHz is the third harmonic of the quarter-wave resonator. Using the circle-fitting method^{24,25}, we extract the Q_i for each of these resonances at different applied powers. Fig. 4b shows Q_i for each resonator from two different samples as well as the reference and con-

trol of one of them for comparison.

We find that all the tested resonators have similar loss in the single-photon limit and follow the same increasing trend with photon number. When the loss is due to two-level systems, Q_i would increase proportionally with frequency. So, the similarity in Q_i between the $\lambda/4$ resonance and its third harmonic suggests that Q_i may be limited by other mechanisms^{23,26–28}. To estimate an upper bound of any loss from NbSe₂, we use the worse case scenario by setting $1/Q_0$ to zero when applying Eqn. 2. In the low-power regime, $Q_i = 260\,000$, corresponding to an upper bound r of $192\,\mu\Omega$.

To estimate the effect of such a dissipative element in a superconducting qubit, we consider a modified transmon¹³ with a resistance r in series with the capacitance, such that the T_1 relaxation time can be estimated by $T_1 = (\omega_q^2 r C_q)^{-1}$ with $\omega_q/2\pi$ and C_q being the frequency and microwave loss of the qubit. This configuration represents a qubit that consists of a parallel plate capacitor made of stacked vdW materials connected to a conventional Josephson junction made of Al. Such a compact and potentially ultra-clean transmon is an immediate application of the materials platform presented here. Using a typical transmon capacitor, $C_q = 60$ fF and $\omega_q = 2\pi \times 5$ GHz, respectively, we find that T_1 can reach nearly $100\,\mu\text{s}$ when limited by r . This conservative estimate confirms that the NbSe₂/Al system can be used to make superconducting quantum devices with long coherence times. We expect that the same fabrication and validation approach can produce high-quality quantum microwave device based on other superconducting vdW materials.

Acknowledgements. We thank B. Hunt and L. Ranzani for useful discussions. This work was supported by Army Research Office under Cooperative Agreement Number W911NF-18-C-0044. A. A. thanks the supplemental support from QISE-NET under NSF DMR-1747426.

A. Appendix

1. Parameters of the quarter-wave resonators

Parameters	Quantity
Length of transmission line, ℓ	$8312\,\mu\text{m}$
Equivalent resonant inductance	$2.2\,\text{nH}$
Equivalent resonant capacitance	$896\,\text{fF}$
Coupling capacitance from the circle fitting	$1.4\,\text{fF}$
Characteristic impedance	$50\,\Omega$

TABLE I. List of quarter-wave resonator parameters.

2. Additional plots

¹R. Barends, J. Kelly, A. Megrant, A. Veitia, D. Sank, E. Jeffrey, T. C. White, J. Mutus, A. G. Fowler, B. Campbell, Y. Chen, Z. Chen, B. Chiaro, A. Dunsworth, C. Neill, P. O'Malley, P. Roushan, A. Vainsencher, J. Wenner, A. N. Korotkov, A. N. Cleland, and J. M. Martinis, "Superconducting

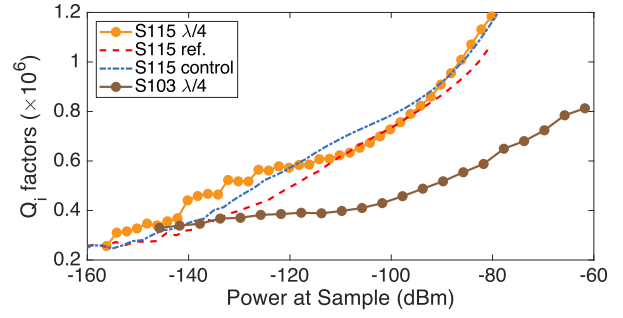


FIG. 5. Internal quality factor vs power applied to the sample for the fundamental mode of different resonators for two devices, as well as the reference and control of one of them for comparison.

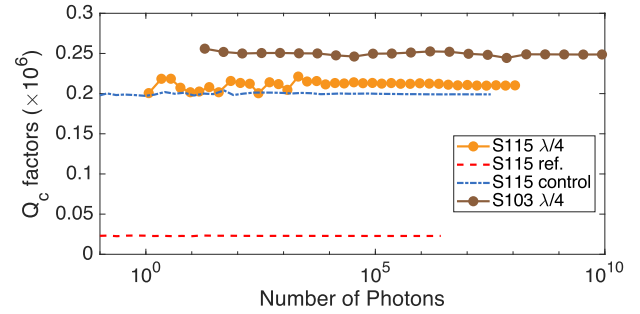


FIG. 6. Coupling quality factor vs the number of photons from the applied power for the fundamental mode of different resonators for two devices, as well as the reference and control of one of them for comparison.

quantum circuits at the surface code threshold for fault tolerance," *Nature* **508**, 500–503 (2014).

²J. M. Chow, J. M. Gambetta, E. Magesan, D. W. Abraham, A. W. Cross, B. R. Johnson, N. A. Masluk, C. A. Ryan, J. A. Smolin, S. J. Srinivasan, and M. Steffen, "Implementing a strand of a scalable fault-tolerant quantum computing fabric," *Nature Communications* **5**, 1–9 (2014).

³M. H. Devoret and R. J. Schoelkopf, "Superconducting Circuits for Quantum Information: An Outlook," *Science* **339**, 1169–1174 (2013).

⁴W. D. Oliver and P. B. Welander, "Materials in superconducting quantum bits," *MRS Bulletin* **38**, 816–825 (2013).

⁵J. I.-J. Wang, D. Rodan-Legrain, L. Bretheau, D. L. Campbell, B. Kannan, D. Kim, M. Kjaergaard, P. Krantz, G. O. Samach, F. Yan, J. L. Yoder, K. Watanabe, T. Taniguchi, T. P. Orlando, S. Gustavsson, P. Jarillo-Herrero, and W. D. Oliver, "Coherent control of a hybrid superconducting circuit made with graphene-based van der Waals heterostructures," *Nature Nanotechnology* **14**, 120–125 (2019).

⁶F. E. Schmidt, M. D. Jenkins, K. Watanabe, T. Taniguchi, and G. A. Steele, "A ballistic graphene superconducting microwave circuit," *Nature Communications* **9**, 4069 (2018).

⁷E. D. Walsh, W. Jung, G.-H. Lee, D. K. Efetov, B.-I. Wu, K. F. Huang, T. A. Ohki, T. Taniguchi, K. Watanabe, P. Kim, D. Englund, and K. C. Fong, "Josephson junction infrared single-photon detector," *Science* **372**, 409–412 (2021).

⁸E. J. Telford, A. Benyamini, D. Rhodes, D. Wang, Y. Jung, A. Zangabadi, K. Watanabe, T. Taniguchi, S. Jia, K. Barmak, A. N. Pasupathy, C. R. Dean, and J. Hone, "Via Method for Lithography Free Contact and Preservation of 2D Materials," *Nano Letters* **18**, 1416 (2018).

⁹A. Benyamini, E. Telford, D. Kennes, D. Wang, A. Williams, K. Watanabe, T. Taniguchi, D. Shahar, J. Hone, C. Dean, *et al.*, "Fragility of the dissipationless state in clean two-dimensional superconductors," *Nature Physics*

- 15**, 947–953 (2019).
- ¹⁰I. Nsanzineza and B. L. T. Plourde, “Trapping a Single Vortex and Reducing Quasiparticles in a Superconducting Resonator,” *Physical Review Letters* **113**, 117002 (2014).
- ¹¹E. Khestanova, J. Birkbeck, M. Zhu, Y. Cao, G. Y. Nano, and 2018, “Unusual Suppression of the Superconducting Energy Gap and Critical Temperature in Atomically Thin NbSe₂,” *Nano Letters* **18**, 2623 (2018).
- ¹²X. Xi, Z. Wang, W. Zhao, J.-H. Park, K. T. Law, H. Berger, L. Forró, J. Shan, and K. F. Mak, “Ising pairing in superconducting NbSe₂ atomic layers,” *Nature Physics* **12**, 139–143 (2016).
- ¹³J. Koch, T. M. Yu, J. Gambetta, A. A. Houck, D. I. Schuster, J. Majer, A. Blais, M. H. Devoret, S. M. Girvin, and R. J. Schoelkopf, “Charge-insensitive qubit design derived from the Cooper pair box,” *Physical Review A* **76**, 42 (2007).
- ¹⁴R. Zhao, S. Park, T. Zhao, M. Bal, C. R. H. McRae, J. Long, and D. P. Pappas, “Merged-Element Transmon,” *Physical Review Applied* **14**, 064006 (2020).
- ¹⁵K. Cicak, D. Li, J. A. Strong, M. S. Allman, F. Altomare, A. J. Sirois, J. D. Whittaker, J. D. Teufel, and R. W. Simmonds, “Low-loss superconducting resonant circuits using vacuum-gap-based microwave components,” *Applied Physics Letters* **96**, 093502 (2010).
- ¹⁶L. Wang, I. Meric, P. Y. Huang, Q. Gao, Y. Gao, H. Tran, T. Taniguchi, K. Watanabe, L. M. Campos, D. A. Muller, J. Guo, P. Kim, J. Hone, K. L. Shepard, and C. R. Dean, “One-Dimensional Electrical Contact to a Two-Dimensional Material,” *Science* **342**, 614–617 (2013).
- ¹⁷Y. Cao, A. Mishchenko, G. L. Yu, E. K. Nano, and A. Lindner, “Quality heterostructures from two-dimensional crystals unstable in air by their assembly in inert atmosphere,” *Nano Letters* **15**, 4914 (2015).
- ¹⁸M. R. Sinko, S. C. de la Barrera, O. Lanes, K. Watanabe, T. Taniguchi, S. Tan, D. Pekker, M. Hatridge, and B. M. Hunt, “Superconducting contact and quantum interference between two-dimensional van der Waals and three-dimensional conventional superconductors,” *Physical Review Materials* **5**, 014001 (2021).
- ¹⁹J. Romijn, T. M. Klapwijk, M. J. Renne, and J. E. Mooij, “Critical pair-breaking current in superconducting aluminum strips far below T_c ,” *Physical Review B* **26**, 3648 (1982).
- ²⁰M. Tinkham, *Introduction to superconductivity*, 2nd ed. (Dover, 2004).
- ²¹G.-H. Lee, S. Kim, S.-H. Jhi, and H.-J. Lee, “Ultimately short ballistic vertical graphene Josephson junctions,” *Nature Communications* **6**, 6181 (2015).
- ²²C. M. Quintana, A. Megrant, Z. Chen, A. Dunsworth, B. Chiaro, R. Barends, B. Campbell, Y. Chen, I. C. Hoi, E. Jeffrey, J. Kelly, J. Y. Mutus, P. J. J. O’malley, C. Neill, P. Roushan, D. Sank, A. Vainsencher, J. Wenner, T. C. White, A. N. Cleland, and J. M. Martinis, “Characterization and reduction of microfabrication-induced decoherence in superconducting quantum circuits,” *Applied Physics Letters* **105**, 062601 (2014).
- ²³C. R. H. McRae, H. Wang, J. Gao, M. R. Vissers, T. Brecht, A. Dunsworth, D. P. Pappas, and J. Mutus, “Materials loss measurements using superconducting microwave resonators,” *Review of Scientific Instruments* **91**, 091101 (2020).
- ²⁴M. S. Khalil, M. J. A. Stoutimore, F. C. Wellstood, and K. D. Osborn, “An analysis method for asymmetric resonator transmission applied to superconducting devices,” *Journal of Applied Physics* **111**, 054510 (2012).
- ²⁵S. Probst, F. B. Song, P. A. Bushev, A. V. Ustinov, and M. Weides, “Efficient and robust analysis of complex scattering data under noise in microwave resonators,” *Review of Scientific Instruments* **86**, 024706 (2015).
- ²⁶U. Patel, I. V. Pechenezhskiy, B. L. T. Plourde, M. G. Vavilov, and R. McDermott, “Phonon-mediated quasiparticle poisoning of superconducting microwave resonators,” *Physical Review B* **96**, 220501 (2017).
- ²⁷L. Grünhaupt, N. Maleeva, S. T. Skacel, M. Calvo, F. Levy-Bertrand, A. V. Ustinov, H. Rotzinger, A. Monfardini, G. Catelani, and I. M. Pop, “Loss Mechanisms and Quasiparticle Dynamics in Superconducting Microwave Resonators Made of Thin-Film Granular Aluminum,” *Physical Review Letters* **121**, 117001 (2018).
- ²⁸M. Göppl, A. Fragner, M. Baur, R. Bianchetti, S. Filipp, J. M. Fink, P. J. Leek, G. Puebla, L. Steffen, and A. Wallraff, “Coplanar waveguide resonators for circuit quantum electrodynamics,” *Journal of Applied Physics* **104**, 113904 (2008).